Lithium insertion mechanism in CoSb3 analysed by 121Sb Mössbauer spectrometry, X-ray: Absorption Spectroscopy and electronic structure calculations

Isabelle Devos, Manfred Womes, Mike Heilemann, Josette Olivier-Fourcade, Jean-Claude Jumas, José Luis Tirado

Lithium insertion mechanism in $CoSb_3$ analysed by ^{121}Sb Mössbauer spectrometry, X-ray absorption spectroscopy and electronic structure calculations

Isabelle Devos,[a] Manfred Womes,[b] Mike Heilemann,[b] Josette Olivier-Fourcade,[b] Jean-Claude Jumas*[b] and José Luis Tirado[c]

[a]*IEMN (UMR 8520 CNRS), Département ISEN, 41 boulevard Vauban, 59046 Lille Cedex, France. E-mail: jumas@univ-montp2.fr*
[b]*LAMMI (UMR 5072 CNRS), Université Montpellier II, CC 15 Place E. Bataillon, 34095 Montpellier Cedex, France*
[c]*Laboratorio de Química Inorgánica, Universidad de Córdoba Campus de Rabanales, C3 Planta 1, 14071 Córdoba, Spain*

The lithium insertion mechanism into the skutterudite-type $CoSb_3$ compound has been studied using X-ray Absorption Near Edge Structure (XANES), ^{121}Sb Mössbauer spectrometry and electronic structure calculations based on the Density Functional Theory (DFT) in the Linear Muffin Tin Orbital (LMTO) framework. ^{121}Sb Mössbauer spectra are in agreement with a progressive restructuring which occurs during the second stage (voltage plateau at 0.6 V). The Mössbauer hyperfine parameters show the formation of Li_3Sb and of a ternary intermediate phase Li_xCoSb_y whose variable composition depends on the insertion conditions. XANES spectra at Sb $L_{I,\ III}$ and Co K edges have been compared to calculated Projected Densities of States (PDOS) of reference compounds containing Co, Sb and Li. This analysis has allowed specification of the restructuring mechanism as a distortion of the $CoSb_6$ octahedral units and confirms the formation of Li_3Sb. The overall characterisations have been interpreted to suggest the first discharge mechanism of restructuring in accordance with the global reaction: $CoSb_3 + (y + z)\ Li \rightarrow (Li_xCo_{1-m}Sb_y + m\ Co + Li_3Sb) \leftrightarrow Li_zCo + y\ Li_3Sb$

Introduction

The currently intensified search for new negative electrode materials for Li-ion rechargeable batteries is reflected by a steadily increasing number of investigations.[1] The main requirements for such active materials are that (i) they readily accept lithium under insertion and (ii) they contain elements which are easily reduced such as Sn or Sb. Among Sb based materials, $CoSb_3$ is a promising candidate due to its skutterudite-type crystal structure, the particularity of which is to exhibit large voids allowing the accommodation of ions.

Actually, $CoSb_3$ or $CoFe_3Sb_{12}$ have been demonstrated to be good precursors of active anode materials for lithium batteries.[2,3] It has been shown that their cycling behaviour is similar to that observed for tin composite oxides (TCO). These TCO have been extensively studied since the work of Idota *et al.*[4] The now generally accepted picture describes the cycling behaviour of TCO as a first discharge which involves a restructuring of the pristine material and irreversible formation of inactive lithium oxide, followed by the reversible formation of Li_xSn alloys ($0 < x < 4.4$).[5–10] Another restructuring mechanism has been shown for 3d metal oxides (CoO, NiO)[11,12] with formation of active Li_2O catalysed by Co^0 nanoparticles. Recently the electrochemical reactivity mechanism of $CoSb_3$ *versus* lithium has been studied by *in-situ* X-ray diffraction, microscopy and magnetic measurements.[13] In this case and as for CoO, the formation of a composite made of Co and Li_3Sb nanograins is observed.

The aim of this work is to analyse the intermediate phases formed during the first discharge in order to understand the chemical process. To this end we combined in this work the use of advanced spectroscopic techniques and theoretical calculations. Our analysis is based on the comparison between the experimental characterisation of several samples and the calculated electronic structure of properly chosen model compounds. Samples are chosen on the first discharge profile in order to be representative of the different stages. ^{121}Sb Mössbauer spectra have been recorded to characterise the antimony electronic structure which is indicative of its oxidation state and chemical environment. Regarding the electronic structure, XANES spectra have been recorded at Sb $L_{I,\ III}$ and Co K edges. These XANES spectra have been interpreted as the ground state electronic structure of the conduction band. As they have to be compared to projected densities of states (PDOS) we have performed electronic structure calculations by using the density functional theory (DFT) in the Linear Muffin Tin Orbital (LMTO) framework. These calculations are realised for well-defined crystalline compounds containing Co, Sb and Li. As a next step we try, using the theoretical conduction bands, to reproduce trends in the evolution of the experimental XANES spectra. Considering the overall characterisations, we are able to suggest a fully coherent picture of the first discharge mechanism.

Experimental

Sample synthesis and electrochemical lithiation

The compounds were prepared by heating stoichiometric quantities of the elements, antimony powder (purity 99.5% Aldrich) and cobalt powder (purity 99.995% Aldrich) in evacuated sealed quartz tubes. The binary sample was heated at 50 °C h^{-1} and maintained for one week at 750 °C. It was then crushed, ground and re-annealed for a further week at 700 °C and finally cooled to room temperature at 10 °C h^{-1}. The material was carefully handled in an argon-filled glove box throughout the

preparation process to prevent unexpected contamination. The purity of the sample was checked by X-ray powder analysis.

For the electrochemical studies, the $CoSb_3$ samples were used as positive electrode materials in Swagelock cells assembled in an argon-filled glove box with Li metal as the negative electrode and 1 M $LiPF_6$ in ethylene carbonate, dimethyl carbonate as the electrolyte. Electrochemical measurements were carried out using a Mac Pile system in galvanostatic mode.

^{121}Sb Mössbauer spectroscopy

^{121}Sb Mössbauer measurements were performed in standard transmission geometry using a ^{121m}Sn in $BaSnO_3$ source of nominal activity 0.5 mCi on a constant acceleration spectrometer. During the measurements, both source and absorber were held at liquid helium temperature to increase the fraction of recoil-free emission and absorption processes. Absorbers at different depth of discharge/charge were prepared in a glove box by carefully opening the cells. The electrode materials containing the active material were mixed with A-Piezon grease and placed on a specific sample holder transparent for γ rays. The velocity scale was calibrated with the standard spectrum of an iron absorber using a ^{57}Co(Rh) source. The zero isomer shift was defined from the spectrum of InSb at 4 K ($\delta = -8.70$ (4) mm s^{-1} relative to the $Ba^{121m}SnO_3$ source). The data were processed using transmission integral analysis software GM5SIT[14] with the Mössbauer source fraction f_s and source line width Γ_s held constant at 0.62 and 1.45 mm s^{-1}, respectively.

X-Ray absorption spectroscopy

XANES was performed at the LURE laboratory (Orsay, France) on the ABS2 experimental station located on the beam line D21 of the DCI storage ring. The accessible energy range of 4 keV to 30 keV allows the study of transition metal K and antimony L edges. $CoSb_3$ and lithiated samples were finely ground and passed through a 5 μm sieve in order to obtain powders of the same particle size. A thin membrane was coated with this powder and protected by a capton film in order to avoid any contact with air. For the lithiated samples, the absorbers were prepared in a glove box. The data collections were carried out at room temperature in transmission mode. The intensities of the incident (I_0) and transmitted (I) beams were measured with two ion chambers. The beam line was equipped with a Si (311) double crystal monochromator for the Co K edge (7700–7800 eV) and with a Si (111) double crystal monochromator for the Sb L_{I-III} edges (4100–4750 eV) allowing a resolution of 0.2 eV and 0.4 eV respectively. Energy calibration was carried out from the standard spectra at the Ni K edge of a high purity Ni foil (8333 eV) and at the Ti K edge of TiO_2 (pre-peak at 4967.5 eV). The XANES spectra were recorded with an energy step width of 0.2 eV and treated by the following procedure, using the ORIGIN™ software.[15] First, the absorption background was subtracted supposing linear behaviour over the whole energy range. Then the spectra were normalised to give the same absorption step amplitude in a range of pure atomic absorption.

Theoretical electronic structure calculations

To understand the trends in the evolution of the experimental XANES spectra from a structural point of view, we compared them with the electronic structures of well defined crystalline compounds containing Co, Sb and Li. From Pearson's Handbooks[16] we chose CoSb (with face sharing $CoSb_6$ octahedra), $CoSb_2$ (in the layered form and in the pyrite form), the hypothetical compound $Li(CoSb_3)_4$ imagined with the 2a sites occupied by lithium atoms (filled skutterudite) in order to be able to reproduce the amorphisation and finally Li_2Sb and Li_3Sb since they are thought to be formed under lithiation.

The electronic structure calculations are carried out within the Density Functional Theory (DFT) framework.[17,18] The DFT is a first principle theory. It determines the ground state properties of an electronic system by the knowledge of its electron density $\rho(r)$. It allows mapping of the many-electron problem on a set of one-electron equations. Then, the total energy of the system is written as a functional of $\rho(r)$. The exchange and correlation energy E_{xc}, which is not known in general, appears in the equations. For purpose of practical calculations, an approximation of this term has to be introduced. The traditional one is the Local Density Approximation (LDA). It is based on the assumption that the relation between E_{xc} and $\rho(r)$ is locally the same as for a free electron gas of identical density, which is quite accurately known. Since projected densities of states (PDOS) are needed for comparison with XANES spectra, we use the ESOCS code.[19] It is based on the use of the Atomic Sphere Approximation (ASA) and a Linear Muffin Tin Orbital (LMTO) expansion of the wave function. The trade off is that an excellent description of the Bloch function is obtained with a minimal basis. The LMTO_ASA expansion allows an easy computation of the projection of densities of states onto atomic sites and a good description of high energy conduction bands. Details of the compounds' electronic structures are reported in Table 1.

Results and discussion

Crystal structure

The $CoSb_3$ crystal structure[20] with the $CoAs_3$ (skutterudite) type crystal structure is based on a bcc lattice (cell constant $a = 9.0305$ Å) with 4 formula units per cell. The unit cell symmetry corresponds to the $Im-3$ space group. Co atoms lie in the 8e position (¼, ¼, ¼) and Sb atoms in the 24g position (0, 0.3351, 0.1602). The skutterudite structure (Fig. 1a) may be viewed as a simple cubic sub-lattice of Co atoms in a basic cell with dimension $a/2$. Six four-membered rings of Sb atoms are inserted in the cubes along the (100), (010) or (001) crystallographic directions, two cubes remaining vacant. The $CoSb_3$ crystal structure (Fig. 1b) may also be considered as corner sharing $CoSb_6$ octahedra which are tilted such that Sb atoms form Sb_4 rings which may be approximated as squares.

Table 1 Identification of the main structures of the valence band of $CoSb_3$ (Fig. 9) and of the conduction bands of $CoSb_3$ (Fig. 10), CoSb (Fig. 11), $CoSb_{2,\ lay}$ (Fig. 12), $CoSb_{2,\ pyr}$ (Fig. 13) and $Li(CoSb_3)_4$ (Fig. 14)

	$CoSb_3$	CoSb	$CoSb_{2,\ lay}$	$CoSb_{2,\ pyr}$	$Li(CoSb_3)_4$
A (−7–−12 eV)	Sb(s)				
B (−6–0 eV)	Co(d)–Sb(p)				
P1 (0–4 eV)	Sb(p)–Co(d)	Sb(p)–Co(d)	Sb_1(p)–Co(d) Sb_2(p)–Co(d)	Sb(p)–Co(d)	Sb(p)–Co(d) Li_{tot}
	Sb(s)–Sb(d)	Sb(s)–Sb(d)	Sb_2(s)–Sb_2(d)	Sb(s)–Sb(d)	
P2 (4–14 eV)	Sb(d)–Co(p)	Sb(d)–Co(p)	Sb_1(d)–Co(p) Sb_2(d)–Co(p)	Sb(d)–Co(p)	Sb(d)–Co(p)

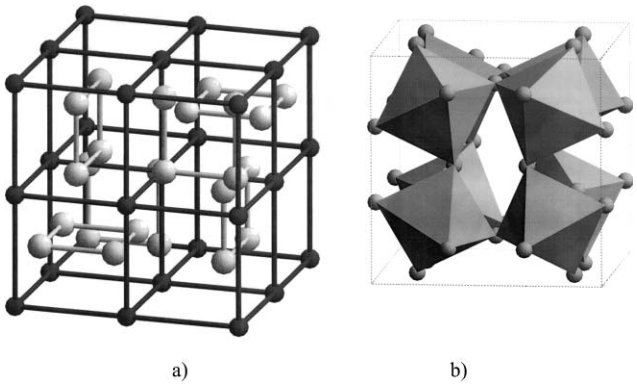

Fig. 1 $CoSb_3$ crystal structure viewed as (a) cubic cobalt (black atoms) units in which antimony (white atoms) rings are inserted or (b) $CoSb_6$ octahedral units.

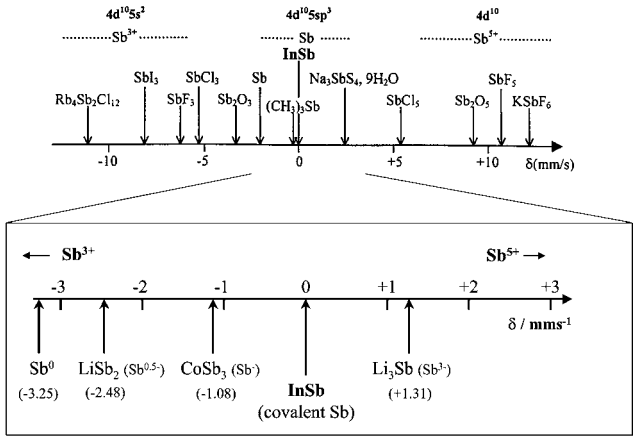

Fig. 3 ^{121}Sb Mössbauer isomer shift scale from reference compounds.

Cycling profile

Fig. 2 shows the first discharge and charge profiles at a 1 Li (per formula unit)/78 h rate for the discharge and at a 1 Li (per formula unit)/42 h rate for the charge. The first discharge shows: i) an abrupt decrease of the voltage potential to 0.6 V for 0.2 Li/$CoSb_3$, ii) a large voltage plateau which characterises a two-phase process up to 8 Li/$CoSb_3$ close to 0.6 V in agreement with a previous study[13] and then iii) a decrease of the potential to 0 V for approximately 9.7 Li/$CoSb_3$. For the first charge the voltage plateau is close to 1.0 V. Several samples have been chosen by interrupting the galvanostatic experiments at different depth of discharge and charge (Fig. 2) in order to identify the intermediate phases formed during the first cycle.

X-Ray diffraction patterns

XRD patterns have been recorded for $CoSb_3$ and samples A_1, A_3 and A_4. The skutterudite structure lines are clearly identified for $CoSb_3$. Their intensity rapidly decreases with ongoing discharge due to progressive amorphisation. They clearly disappear at the end of the first discharge indicating loss of long range order in agreement with previous studies.[2,13] The refinement of the cubic unit cell parameter for $CoSb_3$ leads to a = 9.011 Å, which is in good agreement with the value reported by Kjekshus *et al.*[20] For the other samples, this value is refined to a = 8.995 Å. The difference from the initial value falls within the experimental errors. Thus, no clear expansion of the skutterudite host is detected upon lithiation in agreement with a two-phase process.

Mössbauer spectroscopy

Spectra are mainly characterised by two parameters: the isomer shift (δ) and the quadrupole splitting (Δ). The first corresponds to the peak position on the spectrum. It can be considered as proportional to the Sb (5s) electron density in the valence band.[21,22] δ is thus correlated with the electron configuration and provides an idea of the Sb oxidation state by comparing the measured δ to a reference scale (Fig. 3). The second parameter corresponds to the splitting of the nuclear sub-levels under the influence of the electric field gradient and is thus related to the distortion of the local environment. Its analysis

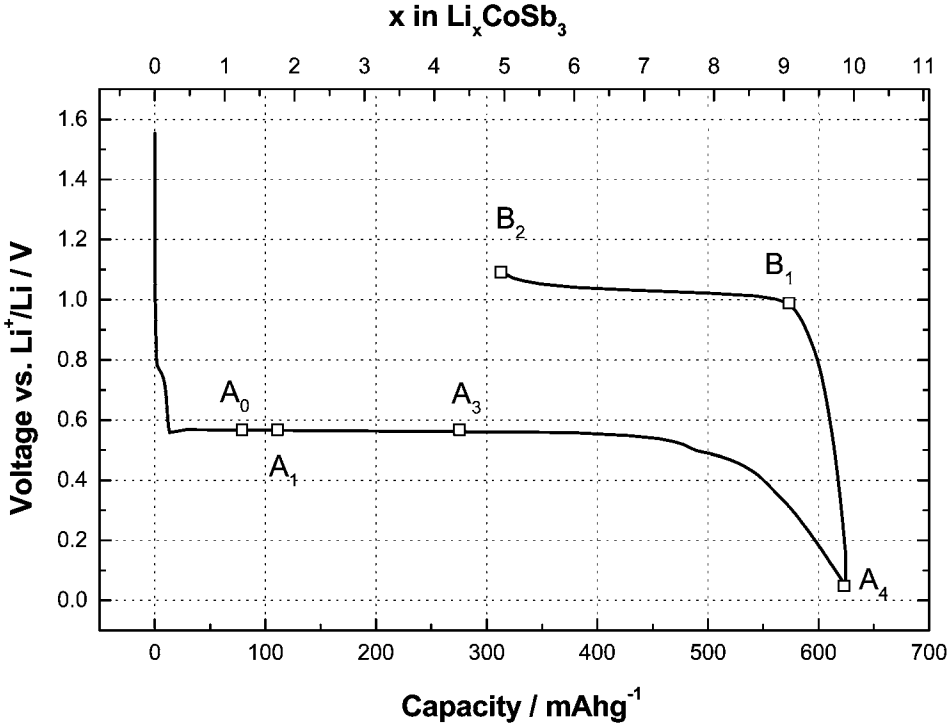

Fig. 2 Cycling profiles of Li/$LiClO_4$ (PC + EC)/$CoSb_3$ cells using 30 and 50 μA currents during charge and discharge respectively. The squares indicate the compositions for which ^{121}Sb Mössbauer (A_1, A_3, A_4, B_1, B_2) and XANES (A_0, A_3) spectra were recorded.

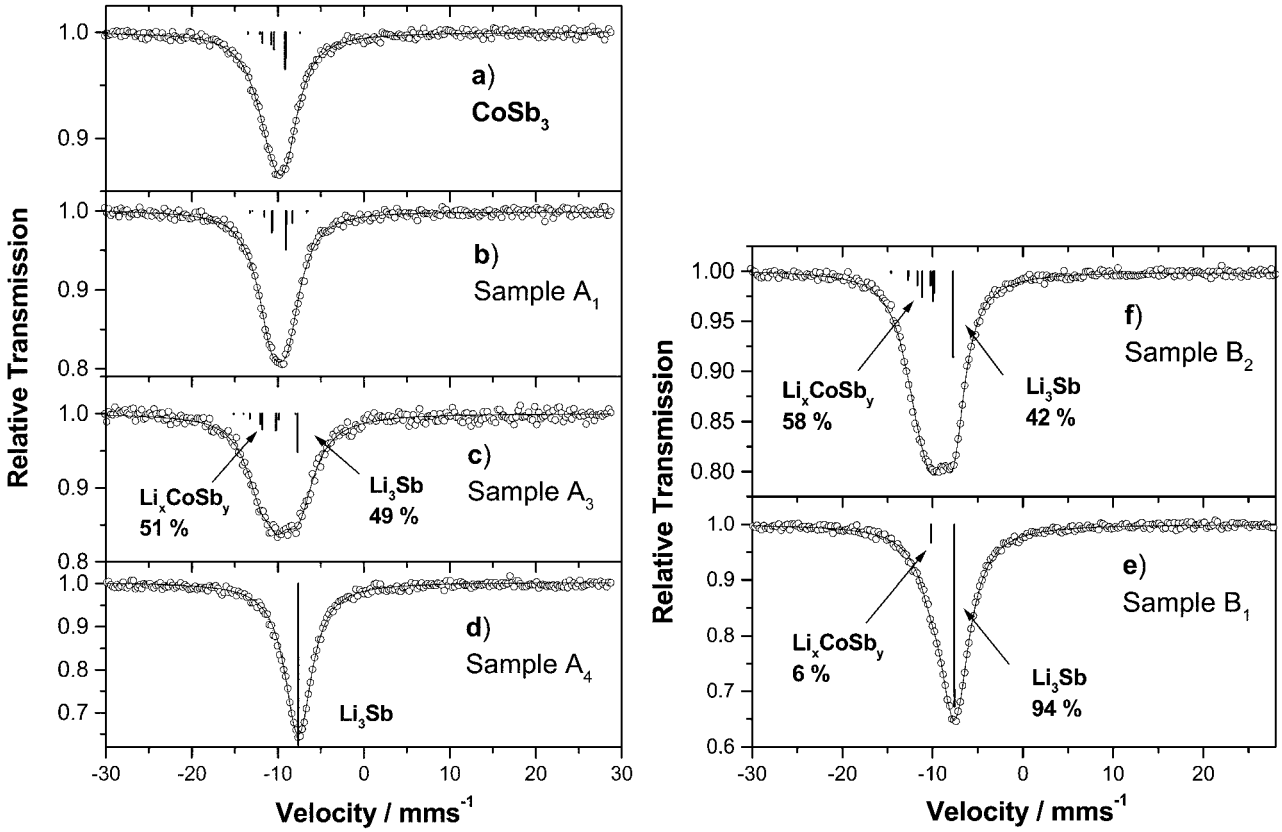

Fig. 4 ^{121}Sb Mössbauer spectra of (a) $CoSb_3$ and $CoSb_3$ based electrodes during cell discharge: (b) A_1 $Li_{1.7}CoSb_3$, (c) A_3 $Li_{4.2}CoSb_3$, (d) A_4 $Li_{10.5}CoSb_3$, and charge: (e) B_1 $Li_{10.5}CoSb_3$, (f) B_2 $Li_{5.0}CoSb_3$.

allows the characterisation of the electron distribution close to the probed nucleus.

Mössbauer spectra are shown in Fig. 4 and the corresponding refined hyperfine parameters are included in Table 2. Concerning $CoSb_3$, the spectral shape and the isomer shift $\delta = -1.08$ (2) mm s^{-1} relative to InSb agree with published data.[20,23] Comparison with the reference isomer shift scale (Fig. 3) shows that this value is intermediate between those observed for elemental Sb and InSb where the Sb (5s) electrons are involved in covalent bonds. The large quadrupole splitting $\Delta = +9.3$ (2) mm s^{-1} and the asymmetry factor $\eta = 0.65$ suggest a strongly distorted environment. It corresponds to the geometrical distortion of the $Sb(Co_2Sb_2)$ tetrahedra and to the chemical difference between the antimony neighbours Co and Sb.

The hyperfine parameters of sample A_1 ($\delta = -1.17$ mm s^{-1} and $\delta = +9.5$ mm s^{-1}) are not modified in comparison to $CoSb_3$ and would be interpreted as a topotactic insertion of 0.2 Li/$CoSb_3$ (filled skutterudite). The spectrum of sample A_3 clearly shows the presence of two components. One of them ($\delta = 1.0$ mm s^{-1} and $\Delta = 0$) can be assigned to Li_3Sb by comparison with the hyperfine parameters of the pure Li_3Sb compound ($\delta = 1.31$ mm s^{-1} and $\Delta = 0$). The other one ($\delta = -2.4$ mm s^{-1} and $\Delta = +10.9$ mm s^{-1}) is assigned to Sb in Li_xCoSb_y with an environment different from the one observed in pristine $CoSb_3$. At the end of the first discharge (sample A_4) the signal of Li_xCoSb_y disappears and only the Li_3Sb signal is present. At the first charge (samples B_1 and B_2) one can observe two components assigned to Li_3Sb and Li_xCoSb_y. The relative contribution of the Li_xCoSb_y sub-spectra increases from 6% (sample B1) to 58% (sample B2). Thus, the reversible cycle takes place between these two phases Li_xCoSb_y and Li_3Sb.

XANES

XANES is particularly well suited to provide insight into the partial densities of unoccupied states. The XANES spectra may be split into two regions, the near edge and the post edge regions (from about 15 eV to 70 eV above the threshold). The second is generally modelled taking into account the multiple scattering of photo excited electrons. The near edge is generally

Table 2 ^{121}Sb Mössbauer data of $CoSb_3$ and $CoSb_3$ based electrodes during cell discharge: A_1 ($Li_{1.7}CoSb_3$), A_3 ($Li_{4.2}CoSb_3$), A_4 ($Li_{10.5}CoSb_3$), and charge: B_1 ($Li_{10.5}CoSb_3$), B_2 ($Li_{5.0}CoSb_3$). δ = isomer shift relative to InSb (−8.70(4) mm s^{-1} relative to the source $Ba^{121m}SnO_3$); Δ = quadrupole splitting; Γ = line width; η = asymmetry parameter; χ^2 = chi-squared and Misfit = comparative goodness of fit criterion which gives the fraction of the experimental signal that remains unfitted

Sample	δ/mm s^{-1}	Δ/mm s^{-1}	Γ/mm s^{-1}	η	C (%)	χ^2	Misfit (%)
$CoSb_3$	−1.08(2)	+9.3(2)	1.61(4)	0.65	100	1.21	0.021
A_1	−1.17(2)	+9.5(3)	1.68(8)	0.91	100	1.11	0.034
A_3	−2.4(2)	+10.9(8)	1.6(3)	0.60	50.7	1.13	0.090
	+1.0(1)	0	2.8(2)		49.3		
A_4	+1.08(1)	0	1.46(4)	—	100	1.07	0.019
B_1	−2.3(1)	0	1.69(6)	—	6.2	1.06	0.022
	+1.08(2)	0	1.69(6)	—	93.8		
B_2	−2.08(2)	+9.7(2)	1.40(4)	—	58.2	1.06	0.022
	+0.96(2)	0	1.40(4)	—	41.8		

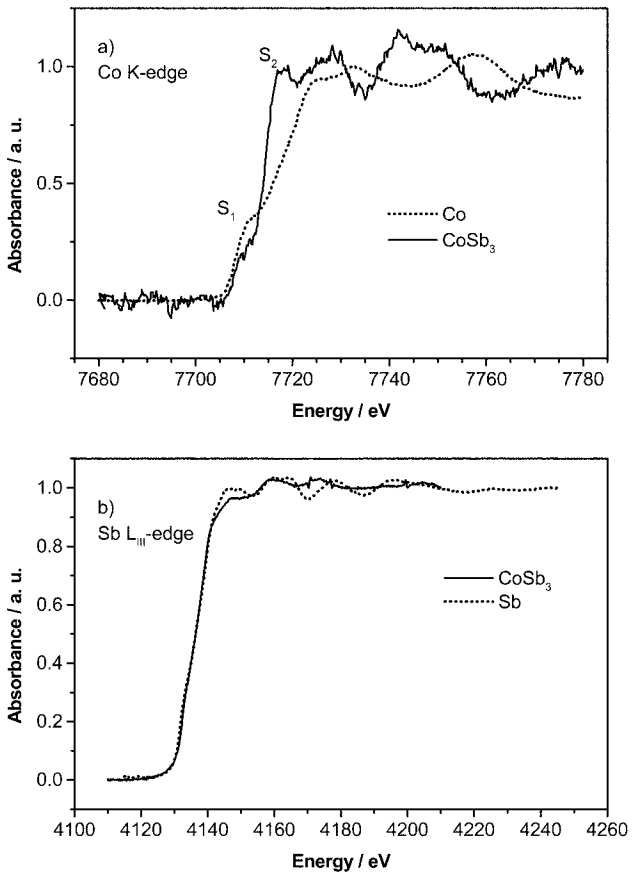

Fig. 5 XANES spectra at the Co K-edge for $CoSb_3$ and Co.

analysed in terms of electronic transitions to empty states, assuming a weak perturbation due to the creation of a core-hole. It has been demonstrated that this is negligible in metals.[24] In $CoSb_3$, we assume that the number of valence electrons on each atom is sufficient to assure good screening of the core-hole allowing in this way an interpretation of the spectra in terms of the electronic ground state of the conduction band.

In all cases the different edges (Co K and L_{I-III} Sb) show two structures labelled S_1 and S_2 in Fig. 5–8 and which will be interpreted from band-structure calculations. A comparison between the Co K-edge spectra of $CoSb_3$ and elemental Co and the Sb L_{III}-edge spectra of $CoSb_3$ and elemental Sb has been made (Fig. 5). From this, we can deduce the following facts:

— the Co K-edge shows a reduced intensity of the pre-peak S_1 around 7709 eV in $CoSb_3$ with respect to Co metal (Fig. 5a) which is due to an Sb–Co charge transfer into unoccupied 3d–4p orbitals of Co. A shift of 5 eV of the main absorption edge S_2 towards lower energies in $CoSb_3$ (7716 eV) with respect to Co metal (7721 eV) is observed. This shift can be explained by the appearance of Co 4p states mixed with Sb 5d states at approximately 6 eV above the Fermi level (see band structure calculations);

— the Sb L_{III}-edge ($2p_{3/2} \rightarrow 5s, 5d$) spectra of $CoSb_3$ and Sb metal (Fig. 5b) are very similar which indicates that the relative charge transfer per Sb atom is rather low while the relative charge transfer per Co atom is more important and thus easily detected.

The superpositions of the XANES spectra for $CoSb_3$ and samples A_0 and A_3 are reported in Fig. 6–8 and the peak positions are summarised in Table 3. The Co K-edge (Fig. 6)

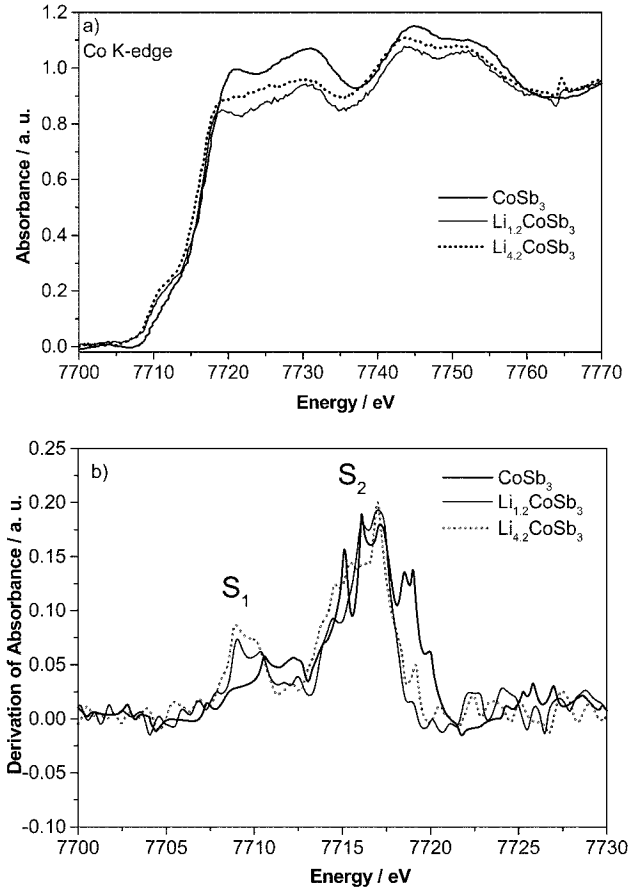

Fig. 6 XANES spectra at the Co K-edge for $CoSb_3$ and samples A_0 ($Li_{1.2}CoSb_3$) and A_3 ($Li_{4.2}CoSb_3$).

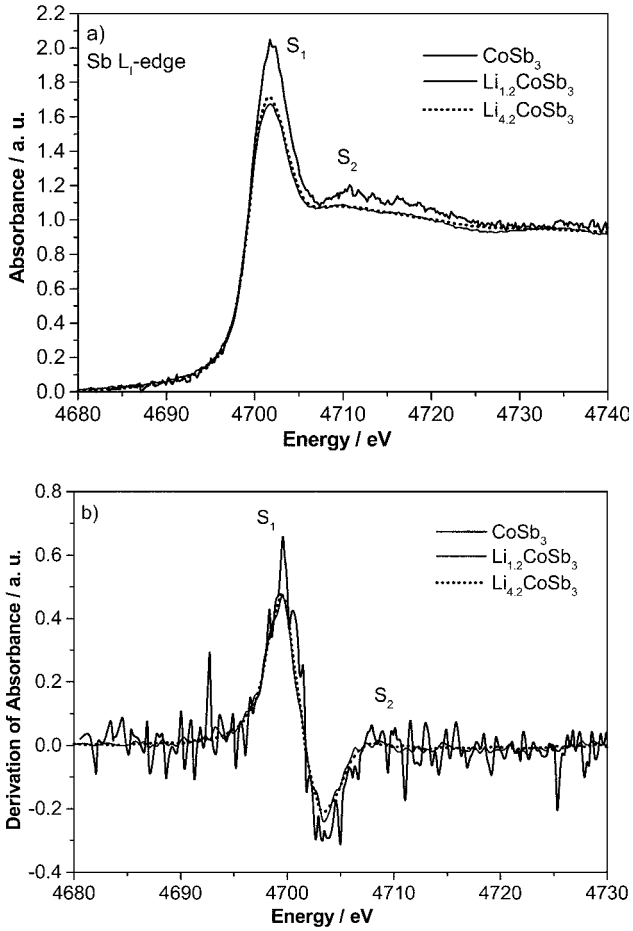

Fig. 7 XANES spectra at the Sb L_I-edge for $CoSb_3$ and samples A_0 ($Li_{1.2}CoSb_3$) and A_3 ($Li_{4.2}CoSb_3$).

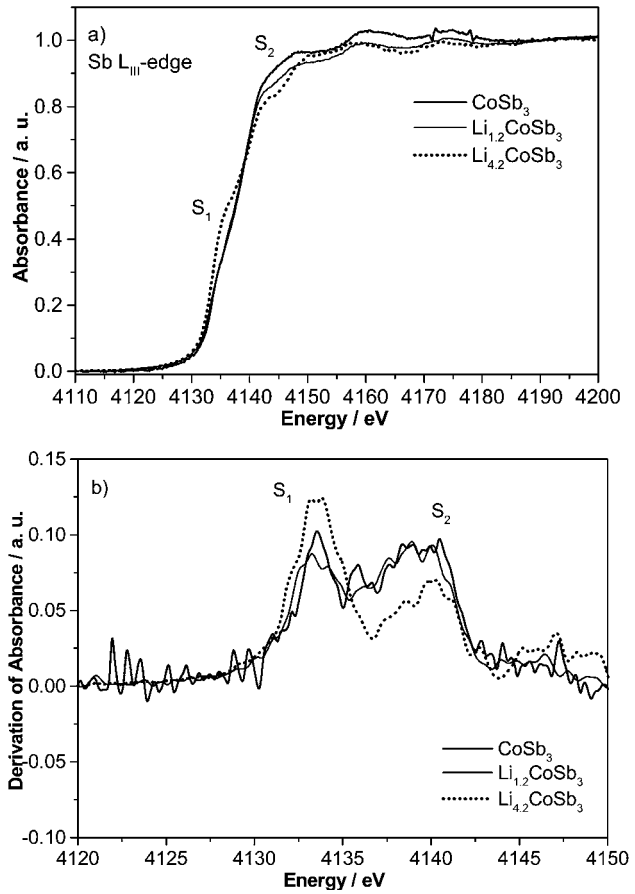

Fig. 8 XANES spectra at the Sb L_{III}-edge for $CoSb_3$ and samples A_0 ($Li_{1.2}CoSb_3$) and A_3 ($Li_{4.2}CoSb_3$).

Table 3 XANES data at the Co K-edge and Sb $L_{I,\ III}$-edges for $CoSb_3$ and $CoSb_3$ based electrodes during cell discharge A_0 ($Li_{1.2}CoSb_3$) and A_3 ($Li_{4.2}CoSb_3$)

		$CoSb_3$	A_0	A_3
Co K-edge	S_1	weak	7709.0 eV	7709.0 eV
	S_2	7716.0	7716.6 eV	7717.0 eV
Sb L_{III}-edge	S_1	weak	weak	4133.6 eV
	S_2	4139.4 eV	4139.4 eV	4140.0 eV
Sb L_I-edge	S_1	4702.1 eV	4701.7 eV	4701.7 eV
	S_2			
FWHM		5.6 eV	5.6 eV	5.7 eV

shows a decrease of the intensity of the S_2 structure when going from $CoSb_3$ to $Li_{1.2}CoSb_3$ which results from the decrease of unoccupied p states. This observation is in agreement with the results of the band structure calculation for $Li(CoSb_3)_4$ which indicates a decrease of Co 4p electron density at 6 eV above the Fermi level. Beyond $Li_{1.2}CoSb_3$ further lithiation leads to the opposite behaviour, increasing the number of vacant Co 4p states. The S_1 pre-edge below the main absorption step is clearly more pronounced after insertion of 4.2 lithium atoms into the host structure. The Sb L_I-edge ($2s \rightarrow 5p$) spectrum of $CoSb_3$ (Fig. 7) is characterised by a white line S_1 (4702 eV) which shows that the p conduction states are localised and a weak S_2 structure (4710 eV). After insertion of 1.2 Li the decrease of the intensity of the S_1 structure and the disappearance of the S_2 structure indicate a reduction of empty Sb 5p states (Fig. 7). This reduction does not continue beyond the 1.2 Li inserted. Concerning the Sb L_{III}-edge (Fig. 8) one can observe for $CoSb_3$ and sample A_0 a very weak shoulder S_1 on the rising edge and the S_2 structure (4139 eV) whose intensity slightly decreases for A_0 indicating that Sb (s, d) states are filled. Between $x = 1.2$ and $x = 4.2$, the Sb L_{III}-edge further

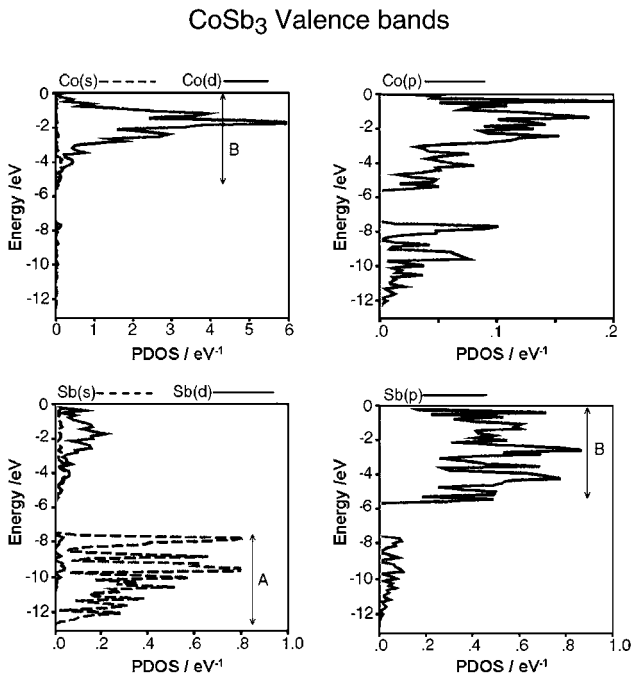

Fig. 9 Calculated $CoSb_3$ valence band PDOS.

loses intensity at 4143 eV (S_2 structure) while a shoulder appears at 4137 eV which seems to indicate a shift of vacant Sb 5d states by approximately 5 eV to lower energies. This fact can be explained by both the Co K-edge, which shows an increasing number of unoccupied Co 4p states, and the Sb L_I-edge which, after an initial lithiation, does not decrease any more. For $Li_{4.2}CoSb_3$ the increase of the intensity of the S_1 structure (Fig. 8) may be indicative of a local order modification.

Theoretical electronic structures of $CoSb_3$ and reference materials

For $CoSb_3$ the PDOS from our calculations (ESOCS) are reported in Fig. 9 and 10. Comparison of these results with a previous analysis of the $CoSb_3$ electronic structure[23] based on

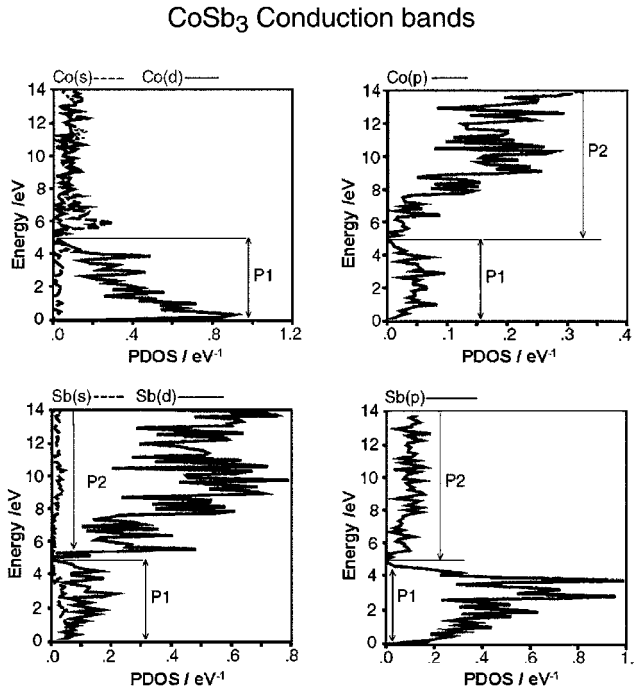

Fig. 10 Calculated $CoSb_3$ conduction band PDOS.

the DOS and PDOS calculated in the CASTEP (DFT-LDA pseudo-potential) and tight binding framework, respectively, shows an overall agreement.

Concerning the valence band, two main structures A and B which are similar in width are found. Structure A is mainly due to Sb (s) states while structure B reflects interactions between Sb (p) and Co (d) states. A deeper analysis of structure A has been realised by comparison with various antimony chalcogenides, in which Sb is characterised by a lone-pair of 5s electrons.[24] In that case, due to the valence Sb (5s) lone pair (the corresponding theoretical population is greater than 1.9 electrons), there is a very weak antibonding contribution of the Sb (5s) states to the conduction band. Nevertheless, the Sb (5s) conducting population in $CoSb_3$ is calculated to be 0.23 electrons, which is more than the maximum 0.1 electron in Sb lone-pair chalcogenides. From these considerations and previous Mössbauer results,[25] we have concluded that the Sb (5s) electrons are delocalised and spread in the conduction band; they do not participate in an antibonding state. With regard to the conduction band, methods correctly describe states within the first 10 eV energy range. The PDOS features are i) in the first 4 eV range a peak labelled P1, whose major character is Sb (p) and Co (d) states [Sb (s) states participate weakly as they are spread in the conduction band, Co (p) states also weakly participate], ii) higher in energy (4–12 eV) , a second peak P2, mainly due to Sb (d) and Co (p) states which we attribute to the octahedral $CoSb_6$ environment. Its energy position is similar to that in the $CoSb_2$ compound where Co is also in an octahedral environment. Its width is consistent with a strong angular distortion of the Co–Sb bonds.

These conduction band features can be attributed to corresponding S_1 and S_2 structures on the XANES spectra. Due to its strong Sb (p) character, peak P1 corresponds beyond any doubt to structure S_1 in the Sb L_I spectrum. Its weak Sb (s, d) character explains the occurrence of the pre-peak S_1 on the Sb L_{III} spectrum and its Co (p, d) character contributes to structure S_1 in the Co K-edge spectrum. Peak P2 corresponds to structure S_2 in the XANES spectra. The energy spacing between P1–P2 (7 eV) is in agreement with those observed between the S_1–S_2 structures (9 eV). The relative intensity of S_2 to S_1 is in agreement with the relative contributions to the PDOS.

Our ESOCS electronic structure is in good agreement with previously published data.[23] This method can be used to go further in the analysis of the lithiation mechanism by calculating the electronic structure of several reference materials: CoSb (Fig. 11) with face sharing $CoSb_6$ octahedra, $CoSb_2$ in the layered form ($CoSb_{2,\ lay}$, Fig. 12) which is highly distorted and in the pyrite form ($CoSb_{2,\ pyr}$, Fig. 13) with perfect $CoSb_6$ octahedra and $CoSb_4$ tetrahedra, $Li(CoSb_3)_4$ (filled skutterudite, Fig. 14) , Li_2Sb and Li_3Sb. The discussion is limited to structures in the conduction band seen in the XANES spectra. The origin of the energy scale is positioned at the bottom of the conduction band for each crystal. The different density scales for the various contributions can be noted.

It is important here to underline several points concerning the conduction bands of these compounds, points which help to better understand the XANES spectra. We first notice that the simple insertion of lithium in the $CoSb_3$ structure does not modify its conduction band (see $Li(CoSb_3)_4$, Fig. 14). The P1 intensity in the Co (p) PDOS is more or less conserved through the $CoSb_x$ family. A possible explanation for the increase of the intensity of the structure S_1 on the Co K-edge XANES spectra would be the formation of Co clusters. For the Sb (p) character of $CoSb_{2,\ lay}$ one may notice that peaks P1 and P2 are no longer distinguished; the PDOS intensity is less in the P1 energy range as it is greater in the P1–P2 energy range (Fig. 12). For the Sb (p) character of CoSb, peak P2 is more structured and exhibits a high intensity sub-structure around 10 eV. As compared to the Sb L_I-edge spectra, the decrease of the intensity of the S_1 structure and the disappearance of the deep set between S1 and S2 are consistent with a strong distortion of the $CoSb_x$ structure (as in $CoSb_{2,\ lay}$). Concerning the Sb (d) character

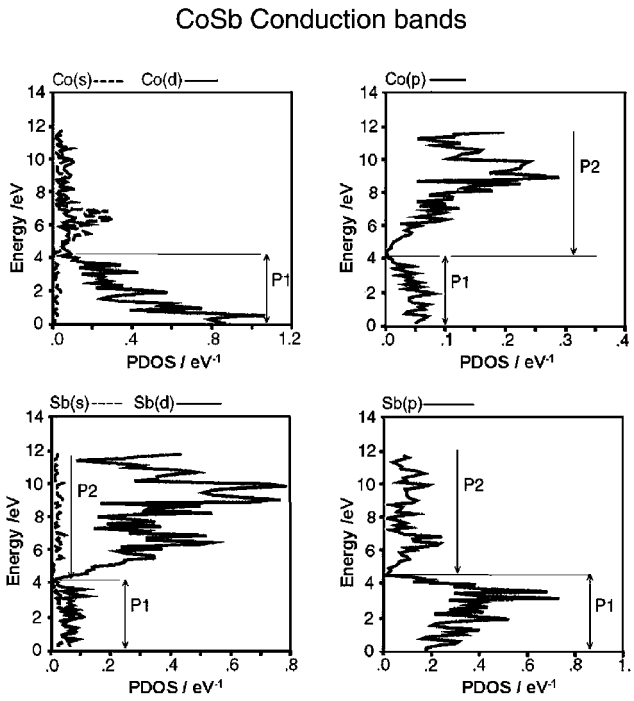

Fig. 11 Calculated CoSb conduction band PDOS.

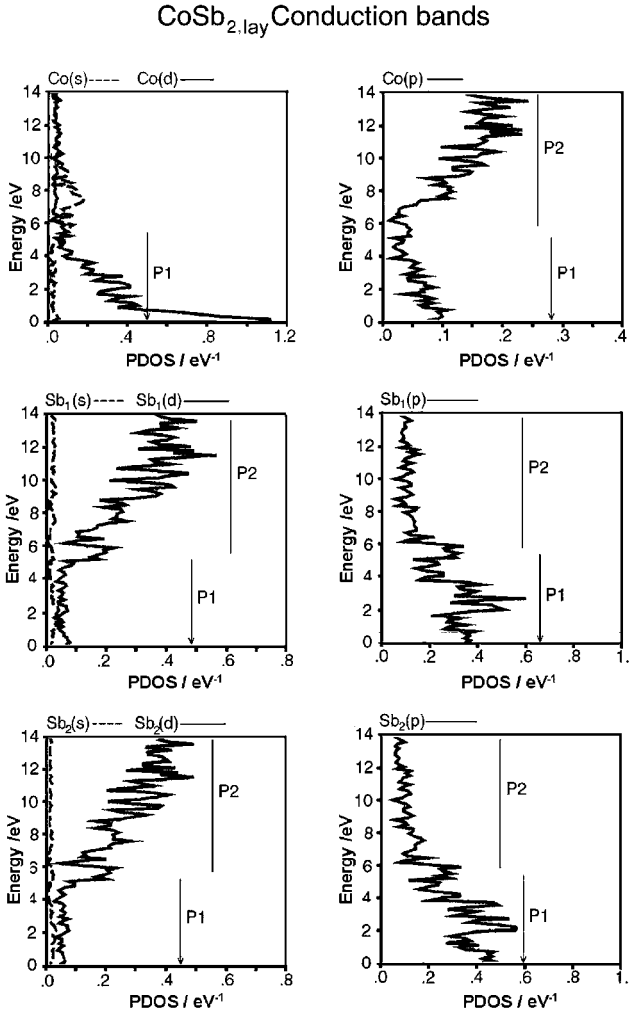

Fig. 12 Calculated $CoSb_{2,\ lay}$ conduction band PDOS.

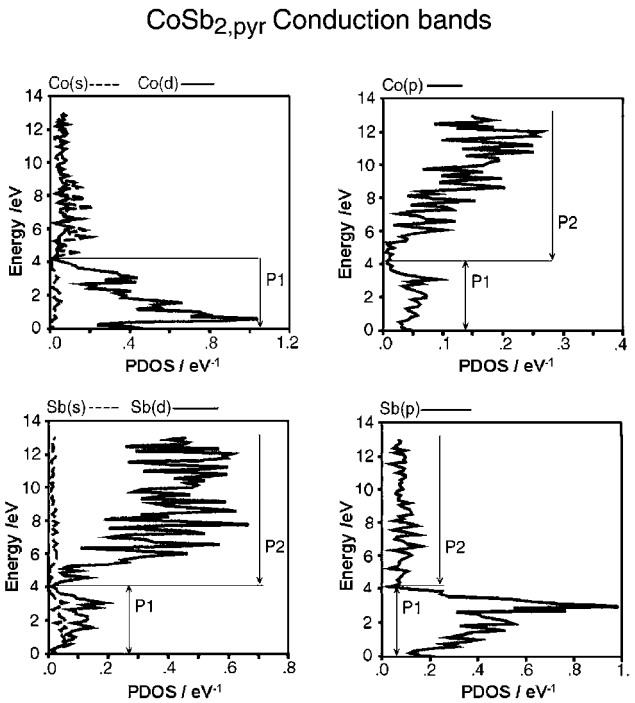

Fig. 13 Calculated $CoSb_{2,\ pyr}$ conduction band PDOS.

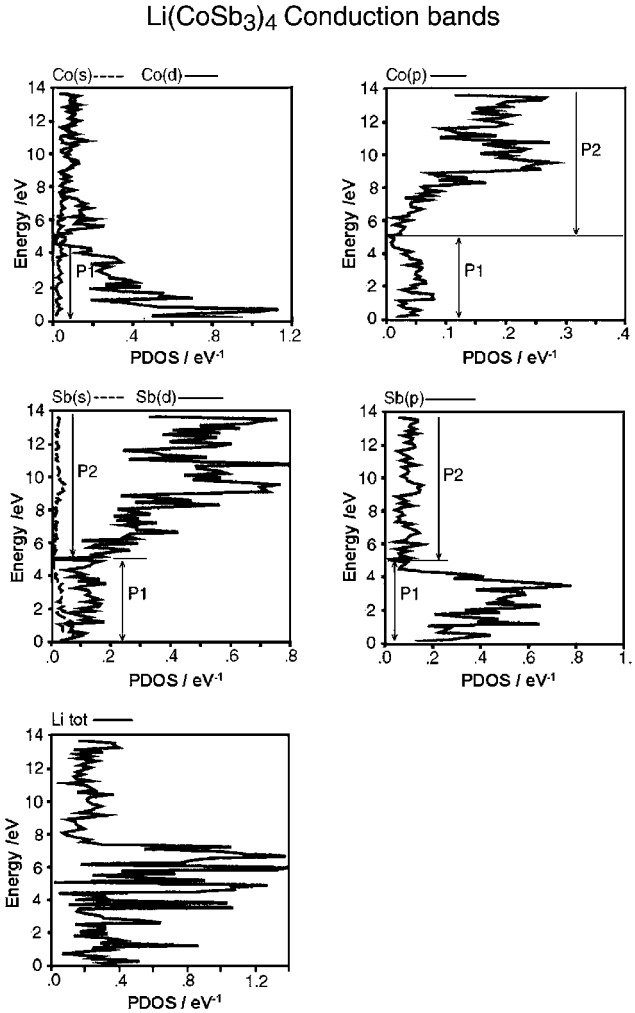

Fig. 14 Calculated $Li(CoSb_3)_4$ conduction band PDOS.

through the $CoSb_x$ series, the intensity of peak P2 is much less for $CoSb_{2,\ lay}$ but its PDOS can not explain the observed energy shift of S_1 (Fig. 8). The simultaneous occurrence of Co–Sb bonds (a $CoSb_{2,\ lay}$ like form) and of Li_3Sb would correspond to a shifted superposition of their L_{III} spectra. This would be able to explain the S_1 shift and the S_2 sub-structures.

First discharge mechanism: restructuring

The first discharge can be divided into three zones which correspond respectively to the insertion of 0.0–0.2 Li/$CoSb_3$, 0.2–8.0 Li/$CoSb_3$ and 8.0–9.7 Li/$CoSb_3$. At the beginning of the insertion, a weak proportion of lithium is introduced as a solid solution in $CoSb_3$ according to the reaction:

$$CoSb_3 + 0.25\ Li \rightarrow Li_{0.25}CoSb_3$$

This new compound ($Li_{0.25}CoSb_3$) can be obtained by filling of the 2a vacant site in the skutterudite structure to make up a "filled skutterudite" ($LiCo_4Sb_{12}$) without modification of the X-ray diffraction pattern and ^{121}Sb Mössbauer spectrum.

The second domain between 0.2 and 8.0 Li/$CoSb_3$ corresponds to a large voltage plateau at about 0.6 V which is characteristic of a two-phase process. X-Ray diffraction data show continuous amorphisation with progressive lithiation, while the host structure of $CoSb_3$ is still observed. No other structure (Li_3Sb, Li_xCoSb_2 and Li_xCoSb) can be identified. This might be due to the fact that the new phases are formed without any long range order. Mössbauer spectra at different steps of lithiation indicate the formation of the Li_3Sb compound between $x = 1.7$ and 4.2 Li and a second compound whose structure and composition is not known (Li_xCoSb_y), characterised by an isomer shift of $\delta = -2.4$ mm s^{-1} and a large quadrupole splitting $\Delta = +10.9$ mms^{-1}. From stoichiometric considerations, the formation of Li_3Sb would result in Sb extrusion from $CoSb_3$. In other respects the XANES spectra at the Co K-edge have shown a slight shift of the S_1 structure towards lower energies in agreement with the possible formation of Co clusters. On the other hand, the Sb L_{III}-edges indicate a more important change in the electronic environment of antimony atoms between the insertion of 1.2 and 4.2 Li, in accordance with the Mössbauer spectra. The general effect of these observations allows us to propose two successive or simultaneous mechanisms for this restructuring plateau at 0.6 V with the two reactions:

$$Li_{0.25}CoSb_3 + x\ Li \rightarrow Li_{0.25+x}Co_{1-x}Sb_3 + x\ Co^0 \quad (1)$$

$$Li_{0.25}CoSb_3 + 3y\ Li \rightarrow Li_{0.25}CoSb_{3-y} + y\ Li_3Sb \quad (2)$$

Note that the intermediate phases ($Li_{0.25+x}Co_{1-x}Sb_3$ for reaction (1) and $Li_{0.25}CoSb_{3-y}$ for reaction (2)) can be represented by the general formula Li_xCoSb_y. At the Sb L_I-edge, the disappearance of a hollow between the S_1 and S_2 structures, interpreted from the band structure calculation of $CoSb_{2,\ lay}$, may be representative of a Li_xCoSb_2 structure-type. This analysis suggests that reaction (1) occurs from the beginning of the voltage plateau when reaction (2) starts between 1.7 and 4.2 Li/$CoSb_3$. The kinetics of these two reactions are probably different and functions of the electrochemical insertion conditions and morphology of the materials. One cannot rule out the formation of a small solid solution domain Li_zCo whose existence has been evidenced previously.[26] The last stage corresponds to the formation of Li_3Sb as is shown by the ^{121}Sb Mössbauer spectrum.

So, the first discharge mechanism can be represented from the global reaction:

$$CoSb_3 + (9 + z)\ Li \rightarrow 3\ Li_3Sb + Li_zCo$$

During the first charge the cycle reversibility occurs between the two phases Li_xCoSb_y and Li_3Sb as is shown in the ^{121}Sb Mössbauer spectra.

Conclusion

We have studied the first discharge mechanism of $CoSb_3$ lithiation. Experimental and theoretical results are combined in order to better understand the electrochemical process. The cycling profile shows three stages for the first discharge. X-Ray diffraction shows that the pristine material is quickly amorphised, although the main diffraction lines of the $CoSb_3$ structure are conserved. ^{121}Sb Mössbauer spectra are in agreement with a progressive reduction of Sb atoms corresponding to the formation of an anionic Sb^{3-} species during the second stage (voltage plateau at 0.6 V). The second phase which is formed during this restructuring corresponds to a ternary compound Li_xCoSb_y which is an intermediate phase, the composition of which depends on the insertion conditions. Regarding the electronic structure, X-ray absorption spectroscopy was carried out at Sb $L_{I,\,III}$ and Co K edges. The spectra were compared to projected densities of states calculated in the DFT-LDA-LMTO framework for well defined crystalline compounds containing Co, Sb and Li. This analysis has allowed us to establish the kind of amorphisation as a distortion of the arrangement of the $CoSb_6$ octahedral units, as in $CoSb_{2,\,lay}$. It is also consistent with the formation of Li_3Sb clusters in a second step. Considering the overall characterisations, we are able to suggest a fully coherent picture of the first discharge mechanism of restructuring according to the global reaction:

$$CoSb_3 + (y + z)\ Li \rightarrow$$
$$(Li_xCo_{1-m}Sb_y + m\ Co + Li_3Sb) \leftrightarrow Li_zCo + y\ Li_3Sb$$

The further cycling is realised between Li_3Sb and $Li_{x+z}Co_{1-m}Sb_y$.

Acknowledgements

The authors acknowledge financial support from the French–Spanish Program PICASSO (contract no. 00755VG) and thank R. Cortes for his help in collecting data on the DCI storage ring at LURE (Orsay, France).

References

1 J. L. Tirado, *Mater. Sci. Eng.*, 2003, **R40**, 103–136.
2 R. Alcántara, F. J. Fernández Madrigal, P. Lavela, J. L. Tirado, J. C. Jumas and J. Olivier-Fourcade, *J. Mater. Chem.*, 1999, **9**, 2517–2521.
3 L. J. Zhang, X. B. Zhao, X. B. Jiang, C. P. Lu and G. S. Cao, *J. Power Sources*, 2001, **94**, 92–96.
4 Y. Idota, T. Kubota, A. Matsufuji, Y. Maekawa and T. Miyasaka, *Science*, 1997, **276**, 1395–1397.
5 I. A. Courtney and J. R. Dahn, *J. Electrochem. Soc.*, 1997, **144**, 2045–2052.
6 J. Chouvin, J. Olivier-Fourcade, J. C. Jumas, B. Simon, Ph. Biensan, F. J. Fernández Madrigal, J. L. Tirado and C. Pérez Vicente, *J. Electroanal. Chem.*, 2000, **494**, 136–146.
7 J. Chouvin, C. Branci, J. Sarradin, J. Olivier-Fourcade, J. C. Jumas, B. Simon and Ph. Biensan, *J. Power Sources*, 1999, **81–82**, 277–281.
8 Y. Wang, J. Sakomoto, C. K. Huang, S. Surampudi and S. G. Greenbraum, *Solid State Ionics*, 1998, **110**, 167–172.
9 G. R. Goward, F. Leroux, W. P. Power, G. Ouvrard, W. Dmowski, T. Egami and L. F. Nazar, *Solid State Lett.*, 1999, **2**, 367–370.
10 I. A. Courtney, J. S. Tse, O. Mao, J. Hafner and J. R. Dahn, *Phys. Rev. B*, 1998, **58**, 15583–15588.
11 P. Poizot, S. Laruelle, S. Grugeon, L. Dupont and J. M. Tarascon, *Nature*, 2000, **407**, 496–499.
12 S. Grugeon, S. Laruelle, R. Herera-Urbini, L. Dupont, P. Poizot and J. M. Tarascon, *J. Electrochem. Soc.*, 2001, **148**, A285–A292.
13 J. M. Tarascon, M. Mocrette, L. Dupont, Y. Chabre, C. Payen, D. Larcher and V. Pralong, *J. Electrochem. Soc.*, 2003, **150**, A732–A741.
14 K. Rubenbauer and T. Birshall, *Hyperfine Interact.*, 1979, **7**, 125–133.
15 Microcal™ Origin™, version 5.0, Microcal Software, Inc., One Roundhouse Plaza, Northampton, MA 01060, USA.
16 P. Villars and L. D. Calvert, *Pearson's Handbooks*, American Society for Metals, Metals Park, OH 44073, 1985.
17 P. Hohenberg and W. Kohn, *Phys. Rev. B*, 1964, **136**, 864–871.
18 W. Kohn and L. J. Sham, *Phys. Rev. A*, 1965, **140**, 1133–1138.
19 Cerius2 User Guide, October 1995, MSI, San Diego, 1995.
20 A. Kjekshus, D. G. Nicholson and T. Rakke, *Acta Chem. Scand.*, 1973, **27**, 1315–1320.
21 I. Lefebvre, M. Lannoo, G. Allan, A. Ibanez, J. Olivier-Fourcade, J. C. Jumas and E. Beaurepaire, *Phys. Rev. Lett.*, 1987, **59**, 2471–2474.
22 P. E. Lippens, *Solid State Commun.*, 2000, **113**, 399–403.
23 I. Lefebvre-Devos, M. Lassalle, X. Wallart, J. Olivier-Fourcade, L. Monconduit and J. C. Jumas, *Phys. Rev. B*, 2001, **63**, 125110–125117.
24 J. E. Müller, O. Jepsen and J. W. Wilkins, *Solid State Commun.*, 1982, **42**, 365–368.
25 J. Olivier-Fourcade, P. E. Lippens, J. C. Jumas, M. Womes, I. Lefebvre, M. Lannoo, J. M. Esteva and R. C. Karnatak, *Eur. J. Solid State Inorg. Chem.*, 1993, **30**, 139–153.
26 M. Bonnemay, E. Levant, G. Bronoel, B. Peslerbe and M. Savy, *Mém. Sci. Rev. Métall.*, 1965, **62**(4), 285–290.